Journal of Alloys and Compounds 735 (2018) 140–149

Contents lists available at ScienceDirect

Journal of Alloys and Compounds

journal homepage: http://www.elsevier.com/locate/jalcom

Dielectric and non-ohmic properties of $Ca_2Cu_2Ti_{4-x}Sn_xO_{12}$ ($0.0 \leq x \leq 4.0$) multiphasic ceramic composites

J.A. Cortés*, G. Cotrim, S. Orrego, A.Z. Simões, M.A. Ramírez

Universidade Estadual Paulista, UNESP, Faculdade de Engenharia de Guaratinguetá, Av. Ariberto Pereira da Cunha, 333, CEP: 12516-410, Guaratinguetá, SP, Brazil

ARTICLE INFO

Article history:
Received 16 April 2017
Received in revised form
30 October 2017
Accepted 7 November 2017
Available online 8 November 2017

Keywords:
CCTO/CTO
(micro)structural characterization
Dielectric and non-linear behavior

ABSTRACT

Multiphasic Sn^{4+} substituted $Ca_2Cu_2Ti_{4-x}Sn_xO_{12}$ ($0.0 \leq x \leq 4.0$) ceramic composites were prepared by solid-state reaction. Their crystalline structure, microstructure, dielectric and non-ohmic properties were investigated. The electric properties and the densification and grain growth mechanisms were strongly influenced by a mixture of multiple phases, as evidenced by X-ray diffraction (XRD). The materials with low Sn^{4+} contents ($x = 0.1$ and 0.2) presented giant dielectric permittivity values, 166381 and 140845 respectively. This should be associated to insulating grain boundaries with activation energies of 0.58 eV and 0.30 eV respectively, as well as conductive grains with activation energies of 0.04 eV and 0.08 eV. On the other hand, samples with higher ionic substitution ($x = 3.8$, 3.9 and 4.0) revealed a new type of tin-based ceramic composites, which exhibit non-linear coefficients (α) of 3.0, 4.0 and 4.0, respectively. A new multiphase ceramic composites with high dielectric performance and non-ohmic properties are summarized.

1. Introduction

In the last decades, the miniaturization of electronic devices has led to an increased demand for materials with enhanced properties in micro-scale level. In this context, giant dielectric materials have been in evidence due to their potential application in microelectronic devices, such as actuators, capacitors and sensors [1–3]. Nowadays, the pseudo-perovskite $CaCu_3Ti_4O_{12}$ (CCTO) which exhibits non-ohmic behavior and dielectric constant values of about 10^4 - 10^6 in a considerable range of frequencies (1 Hz - 1 MHz) and temperatures (from − 238 °C to 1000 °C), has been extensively investigated [4–7]. The high dielectric loss (tanδ) of CCTO is undesirable for many practical applications, therefore much work is being conducted to minimize such losses [5–10]. Doping or substitution of metallic ions in the CCTO lattice are effective strategies to decrease the dielectric loss [11–13]. Ribeiro et al. have reported that the substitution of Sn^{4+} into Ti^{4+} sites decreased tanδ and the dielectric permittivity, but improved the non-ohmic behavior [14]. I n addition, reduced values of dielectric loss have also been observed by the substitution of Sr^{2+} into Ca^{2+} [15,16] or Zn^{2+} into Cu^{2+} sites in single phase CCTO [17,18]. Guoping Du et al. shown that the Y^{3+} in the A-site and the Al^{3+} in the B-site produce a considerable decay in the dielectric loss [19]. Chung et al. have shown that $CaCu_3Ti_4O_{12}$ has an outstanding nonlinear *I-V* characteristic, which is greater than the one associated to the traditional ZnO-based varistors [20,21]. A different approach focused on the synthesis of $CaCu_3Ti_4O_{12}/CaTiO_3$ (CCTO/CTO) ceramic composites, with nominal chemical formula of $Ca_2Cu_2Ti_4O_{12}$, have shown high values of dielectric permittivity with low dielectric loss when compared to single phase CCTO [17]. This system has been also investigated due to the huge improvement in the non-ohmic behavior [22]. Thongbay et al. have shown that the ionic substitution of Zr^{4+} into Ti^{4+} sites in CCTO/CTO ceramic composites decreased the dielectric loss [23]. ZnO-based polycrystalline materials have already been studied by Ramirez et al., showing good non-ohmic response [24,25]. These results could indicate that the ionic substitution may be an effective strategy to obtain multiphasic ceramics with interesting non-ohmic properties.

The novelty of this research concerns the investigation of the impact of Sn substitution for Ti on the microstructural, dielectric and non-ohmic properties of CCTO-based ceramics. A systematic study was carried out using chemical compositions described as $Ca_2Cu_2Ti_{4-x}Sn_xO_{12}$ ($0.0 \leq x \leq 4.0$) prepared by the solid-state reaction method. The relationships between composition, dielectric

* Corresponding author.
E-mail address: joalcosu.nal@gmail.com (J.A. Cortés).

https://doi.org/10.1016/j.jallcom.2017.11.089
0925-8388/

and non-ohmic behavior, and the mechanisms responsible for the unusual electrical properties in this multiphase system were established.

2. Experimental procedure

2.1. Synthesis

Polycrystalline ceramic composites, with nominal chemical formula $Ca_2Cu_2Ti_{4-x}Sn_xO_{12}$ with x = 0.0, 0.1, 0.2, 2.0, 3.8, 3.9 and 4.0 were prepared by the solid-state reaction method. Analytical grade $CaCO_3$ (Aldrich, 99.99%), CuO (Aldrich, 99.99%), TiO_2 (Aldrich, 99.99%) and SnO_2 (Aldrich, 99.99%) powders were used to prepare all the samples. The raw materials were mixed and milled in isopropanol suspension for 24 h with yttrium-stabilized zirconia balls inside a polyethylene bottle. The product was dried at 100 °C for 12 h and annealed at 950 °C for 12 h in air using a heating rate of 5 °C/min. The calcination temperature was determined by thermogravimetric analysis (TG) and differential thermal analysis (DTA) (Netzsch, Model STA 409). After the heat treatment, the resulting powder was milled once again using the same conditions for 12 h. The powders were uniaxially pressed into disks 12 mm diameter and 1.2 mm thick, using a pressure of 140 MPa and polyvinyl alcohol (PVA) as a binder. The samples were annealed at 500 °C for 1 h to remove the PVA with a heating rate of 1 °C/min; then, the temperature was increased for sintering the pellets. The sintering temperatures were determined by optical dilatometry (OD) (Hesse Instruments, Model EM-201). Two different sintering temperatures were studied in order to reach similar densities: 1150 °C for 2 h, for Sn^{4+} substitutions of x = 0.0, 0.1, 0.2 and 2.0, and 1400 °C for 2 h, for Sn^{4+} substitutions of x = 3.8, 3.9 and 4.0. Heating and cooling rates of 5 °C/min were used for all the heat treatments.

2.2. Characterization

Phase analysis of the powders and pellets were performed by X-ray diffraction (XRD) (RIGAKU, model RINT2000), operating in the reflection mode with a CuKα source and over the 2θ range of 20°–80°, with a step size of 0.02°. The crystalline structure of the phases was identified based on the Joint Committee on Powder Diffraction Standards files (JCPDS) and compared with the respective simulations, which were made with the software Powder-cell 2.4®. In order to reveal the microstructure, field emission scanning electron microscope (FE-SEM) (JEOL, Model 7500F) was employed. The samples were prepared according to the following procedure: The disks were immersed in cold acrylic resin, then ground using a set of sandpapers with gradual finer abrasives. Alumina suspension with particle size of 1 μm was until a mirrored surface was obtained. Later, the pellets were thermally treated at a 100 °C below the sintering temperature. for 30 min. The average grain sizes were determined by the linear intercept method. The specific mass and pore size distributions of the samples were estimated using the Archimedes method and mercury porosimetry (Micromeritics, Model Auto Pore IV), respectively. Dielectric and non-ohmic properties were studied using an $Au/Ca_2Cu_2Ti_{4-x}Sn_xO_{12}/Au$ capacitor structure. Gold electrodes were deposited on the flat surfaces of the pellets by DC sputtering at room temperature. Dielectric permittivity (ε′) and dielectric loss (tanδ) were obtained by impedance spectroscopy measurements in a frequency response analyzer (Metrohm Autolab B.V., model PGSTAT128N), in a range from 1 Hz to 1 MHz (voltage amplitude of 100 mV). The activation energy (E_a) was obtained of the slope of the conductivity graph as a function of temperature [26,27]. The AC conductivity was obtained by the following equation.

$$\sigma_{AC} = \omega\varepsilon_0\varepsilon' \tan\delta = \omega\varepsilon_0\varepsilon'' \quad (1)$$

where ωis the angular frequency, ε_0 the vacuum permittivity, ε' corresponds to the permittivity of the material and tan δ the dielectric loss. The E_a for the grain boundaries and for the grains were calculated using the following equations.

$$\sigma_{gb} = \frac{d}{R_{gb}A} \quad (2)$$

$$\sigma_b = \frac{d}{R_bA} \quad (3)$$

where d is the thickness, A the area of the electrode, R_{gb} is the grain boundary resistance and R_b, the grain resistance.

Finally, current-voltage measurements were performed using a stabilized high voltage source-measure unit (Keithley, Model 237), with a 0.5 s delay between the measurements. The non-linearity coefficient (α), leakage current (I_L) and breakdown electric field (E_b) were measured according to the procedures described in the literature [28,29].

3. Results and discussion

Fig. 1a–b illustrate the TG/DTA curves for all investigated samples. As can be seen, the first stage (from room temperature to

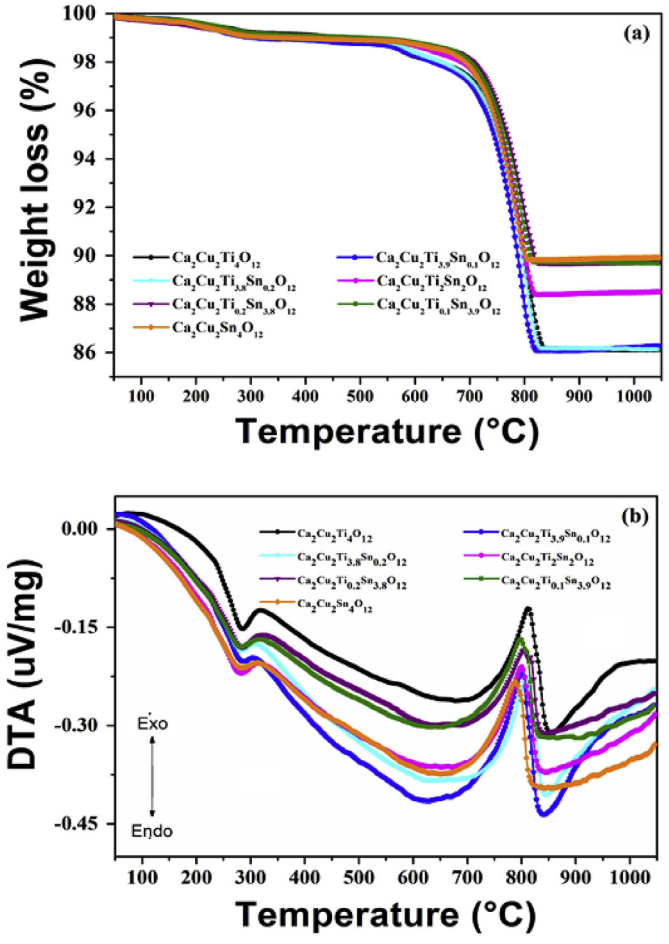

Fig. 1. (a) Differential thermal analysis (DTA) (b) Thermogravimetric analysis (TG) $Ca_2Cu_2Ti_{4-x}Sn_xO_{12}$ powders for Sn^{4+} substitutions.

250 °C) corresponds to a small weight loss which can be related to adsorbed water, while the second stage evidenced by an exothermic peak in the DTA curve at around 800 °C, can be associated to the CO_2 release, due to the carbonate decomposition followed by the phase crystallization [30]. After carbonate decomposition, around 850 °C, no weight loss can be observed, evidencing the formation of stable phases.

Fig. 2a-g shows the evolution of the XRD patterns of calcinated $Ca_2Cu_2Ti_{4-x}Sn_xO_{12}$ powders. For the sample with x = 0.0 (Fig. 2a), the diffraction peaks were indexed to the $CaCu_3Ti_4O_{12}$ (JCDPS #75-1149) and $CaTiO_3$ (JCPDS #65-3287) perovskite phases while for the low ionic substitutions x = 0.1 (Fig. 2b) and x = 0.2 (Fig. 2c), peaks related to the SnO_2 rutile phase (JCPDS #72-1147) are evident. For high Sn^{4+} substituted samples (x = 3.8, 3.9 and 4.0) (Fig. 1e–g), SnO_2 (JCPDS #72-1147), $CaSnO_3$ (JCPDS #75-179) and CuO (JCPDS #65-2309) phases could be detected. We can expect that the crystalline $CaSnO_3$ phase is a consequence of the reaction between $CaCO_3$ and SnO_2. Whose similar results were found for the $BaSnO_3$ system, as shown by Huang et al. [31]. In the intermediate tin substituted range with x = 2.0 (Fig. 2d), the coexistence of all the previously mentioned phases was observed.

Optical dilatometry analysis was an important tool to monitor the influence of the Sn^{4+} substitution on the shrinkage behavior during sintering, as shown in Fig. 3. As can be seen, the initial sintering stage is similar for all the samples, starting around 900 °C, while for the intermediate and final sintering stages differ, according to the ionic substitution. For samples with x = 0.0 and low Sn^{4+} substitutions (x = 0.1 and x = 0.2), the changes in dimensions due to the sintering process are similar. One can also notice that the maximum shrinkage is reached at around 1150 °C, followed by the onset of liquid phase formation. On the other hand, for high Sn^{4+} substituted samples (x = 3.8, 3.9 and 4.0) a noticeable increase in the final densification stage temperature (approximately 200 °C) was observed and no liquid phase formation could be detected up to 1400 °C. Based on these results and on literature data [31–33], two different sintering temperatures were chosen: 1150 °C, for Sn^{4+} substitutions up to x = 2.0, and 1400 °C for Sn^{4+} substitutions higher than x = 2.0. As a consequence, similar shrinkage rates and porosities were observed.

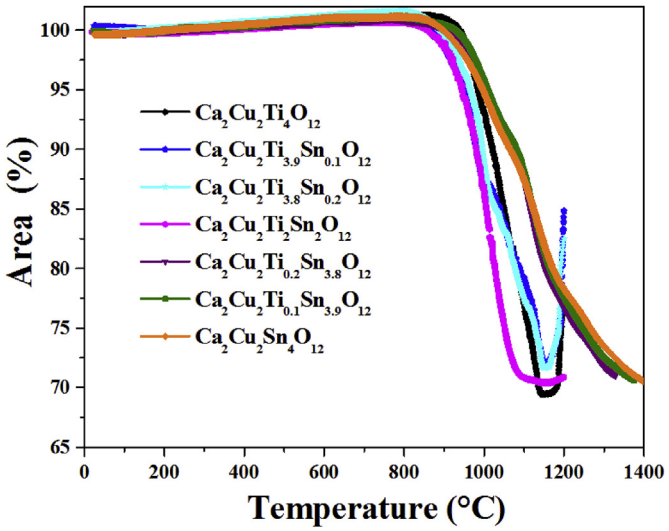

Fig. 3. Optical dilatometric curves of $Ca_2Cu_2Ti_{4-x}Sn_xO_{12}$ samples.

Fig. 4a-g shows the evolution of the XRD patterns of $Ca_2Cu_2Ti_{4-x}Sn_xO_{12}$ for the sintered pellets. The x = 0.0 sample (Fig. 3) has shown the presence of peaks related to the TiO_2 phase (JCPDS #84-1283). This can be attributed to the sintering temperature, which was 50 °C above the typical sintering temperature used for these

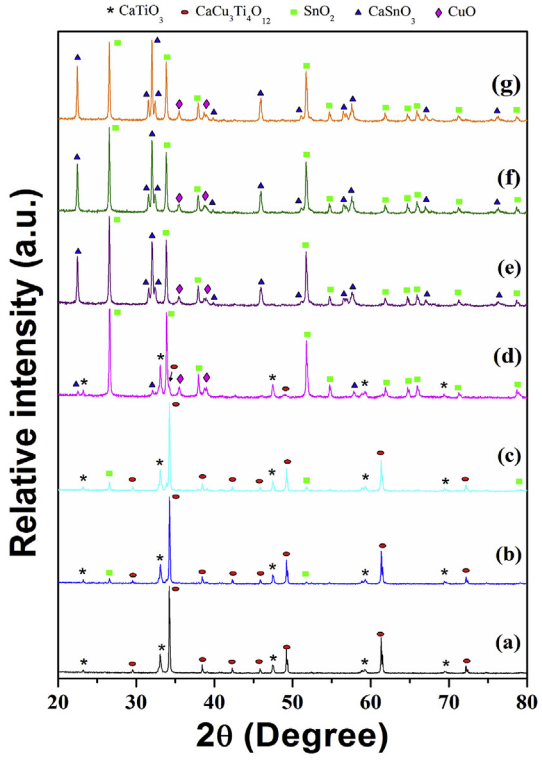

Fig. 2. XRD patterns of $Ca_2Cu_2Ti_{4-x}Sn_xO_{12}$ powders for Sn^{4+} substitution of (a) x = 0.0 (b) x = 0.1; (c) x = 0.2; (d) x 2.0; (e) x = 3.8; (f) x = 3.9; (g) x = 4.0.

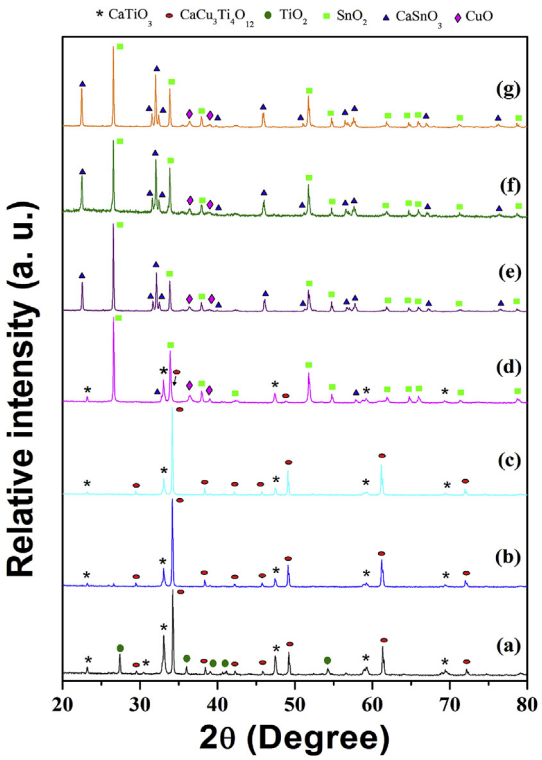

Fig. 4. XRD patterns of $Ca_2Cu_2Ti_{4-x}Sn_xO_{12}$ pellets with Sn^{4+} substitution of (a) x = 0.0 (b) x = 0.1; (c) x = 0.2; (d) x 2.0; (e) x = 3.8; (f) x = 3.9; (g) x = 4.0.

ceramic composites. This result is in agreement with data reported in the literature [34,35] showing that CCTO decomposes into TiO_2, Cu_2O, and $CaTiO_3$ phases when sintered at temperatures above 1100 °C. For low Sn^{4+} substitutions (x = 0.1 and x = 0.2), (Fig. 3), no peaks related to the SnO_2 phase were evident, indicating that the sintering process allows to diffuse Sn^{4+} ions into the CCTO lattice. On the other hand, for high Sn^{4+} substituted samples (Fig. 4D–g) the same phases found in the calcinated powders were noted, indicating that the sintering process mainly leads to densification (see Table 1), without any significant phase changes. These results corroborate with those from the structure simulation shown in Table S1, where the lattice parameters of the CCTO phase increased, while those for the CTO phase remained constant after Sn^{4+} addition. Jumpatam et al. [36] have observed by energy-dispersive X-ray spectroscopy that the Sn^{4+} substitution is more effective into the CCTO lattice than in the CTO lattice, in agreement with our results for low Sn^{4+} substituted samples (x = 0.1 and x = 0.2). For high Sn^{4+} substituted samples (x = 3.8, 3.9 and 4.0) less Ti^{4+} is within the structure, leading to the formation of other stable phases, such as $CaSnO_3$, CuO and SnO_2.

Fig. 5a-g shows the FE-SEM micrographs of $Ca_2Cu_2Ti_{4-x}Sn_xO_{12}$ ceramic composites with different levels of Sn^{4+} content. It is clearly observed that the Sn^{4+} substitution induces grain growth up to x = 2.00. The grains become smaller as the Sn^{4+} content is higher than x = 2.0. It is proposed that the CuO phase favors the grain growth when the samples are sintered at 1150 °C, which is closer to the melting temperature of such oxide (≅ 1080 °C). On the other hand, for the samples sintered at 1400 °C the CuO phase volatilizes, yielding a decrease of the grain size [37]. Besides that, the porosity decreased continuously with the increase in the ionic substitution, as shown in Table 1. Modeling the densification and grain growth is complicated because more than one mass transport mechanism contributes to the changes in the ceramic microstructure [38]. Although the soaking time was kept constant, two sintering temperatures were used, and the final results were similar in terms of shrinkage. This indicates that the presence of other phases during the sintering process play an important role in the diffusion of oxygen vacancies and cupper in the composite, leading to different mass transport mechanisms, and consequently, to different densification and grain growth processes. In the CCTO/CTO, the CuO phase was also reported at the triple point grain boundary regions [35,39]. This phase, when present in the grain boundaries, may inhibits the boundary movement, acting as an inclusion and exerting a drag force which reduces the effective mobility, delaying the grain growth of the CCTO and CTO phases. Therefore, the dominant sintering mechanism is controlled by the cupper oxide from CCTO and may be related to the lattice diffusion process, as previously reported [35]. Comparing to the x = 0.0 sample, low Sn^{4+} substituted samples (x = 0.1 and 0.2) has led to densification and grain growth processes as the main sintering mechanism. On the other hand, it is well-known that the sintering behavior of SnO_2/CuO compounds above 1100 °C is controlled by the liquid phase mechanisms [40,41]. As shown, for high Sn^{4+} substituted samples (x = 3.8; x = 3.9 and x = 4.0), the presence of CuO and SnO_2 phases are affecting the shrinkage behavior of the samples [41]. For the sample with the Sn^{4+} substitution of x = 2.0, mainly composed by SnO_2 and CuO, the final densification stage reached around 950 °C (Fig. 2), which is near to the eutectic temperature of SnO_2/CuO compounds [42]. The largest grain size was related to the high isothermal sintering temperature (1150 °C) and the fastest shrinkage rate, respectively. On the other hand, the samples with Sn^{4+} substitution above x = 2.0 were mainly composed by SnO_2, $CaSnO_3$ and CuO phases. In these samples, the densification process occurs slowly and at high temperatures, due to the competition between the grain growth of the SnO_2 and $CaSnO_3$ phases. Also, the liquid phase composed of CuO reduces the porosity and, mainly, the grain growth of both phases [38].

Table 1
Average specific mass, average grain size and porosity for $Ca_2Cu_2Ti_{4-x}Sn_xO_{12}$ ceramic composites.

Samples Sn^{4+} substitution	Average specific mass (g/cm^3)	Average grain size (μm) ±0.01 μm	Porosity (%)
x = 0.0	4.23	0.75	5.40
x = 0.1	4.35	1.88	3.50
x = 0.2	4.41	1.14	3.80
x = 2.0	5.22	4.17	3.70
x = 3.8	5.81	3.60	1.50
x = 3.9	5.79	2.78	0.60
x = 4.0	5.75	2.53	0.30

Fig. 6 shows the frequency dependence of the dielectric permittivity and the dielectric loss factor of the ceramic composites between 10^0 and 10^6 Hz, at room temperature. The x = 0.0 sample presents a stable plateau in a broad frequency range (10^4–10^6 Hz), with values similar to the ones in the published literature [42,43]. A huge improvement in the dielectric permittivity with a decrease in the dielectric loss were observed for the ceramic composites with low Sn^{4+} substituted samples (x = 0.1 and x = 0.2) in a frequency range from 10^2 to just below 10^5. The losses measured for these two samples are lower than the values for sample x = 0.00. This can be explained by a hopping polarization mechanism, taking place at frequency values around 1 kHz, associated with the charge interaction between electrons and oxygen vacancies inside the grains [44,45]. For the high Sn^{4+} substituted samples (x = 3.8, 3.9 and 4.0), there was a large decrease in the dielectric permittivity and an increase in the dielectric loss. However, as shown in Table 2, all samples had an increase in the dielectric loss when compared to the sample with x = 0.0 at 10 kHz. This could be ascribed to the dipolar polarization mechanism, which is commonly found in this frequency range. The permittivity values for samples with x = 0.1 and x = 0.2 (Table 2) were large when compared to the ones already reported in the literature for CCTO and CCTO/CTO phases [46,47]. The main changes in dielectric permittivity of the Sn^{4+} substituted CCTO/CTO composites have being explained by different researchers. The dielectric permittivity of CCTO is related its grain size, and larger grains result in higher dielectric permittivity [48]. The huge grains contain more defects, which will lead to more carriers; and the chemical and physical properties would be no uniform in contrast to the small grains, which eventually result in more internal barrier layer capacitor (IBLC) in CCTO improving the dielectric permittivity [49,50]. As previously shown in the XRD patterns, lower Sn^{4+} substituted samples (x = 0.1 and x = 0.2) moves into the solid solution within the grains of CCTO/CTO composite, rather than locating at the grain boundaries, which will change the physical and chemical properties of the grains, changing the dielectric permittivity. As the amount of Sn^{4+} is increased, the appearances of other phases as well as the increase of the average grain size produce a decrease in the dielectric permittivity. The frequency dependence of dielectric loss factor (tan δ) of the samples is shown in Fig. 6b. Such behavior observed for low Sn^{4+} substituted samples (x = 0.1 and x = 0.2) reveals different polarization mechanisms with frequency changes which is a reflex of mixture of phases with different electrical conductivities [51]. For high Sn^{4+} substituted samples (x = 3.8, 3.9 and 4.0) a strong decay is indicative of a conductive behavior. The sample with x = 2.0 shows relaxation behavior up to 10^5 Hz due the coexistence of multiple phases.

Fig. 7a illustrates AC conductivity plots in the frequency function. Having in mind that AC conductivity is proportional to the

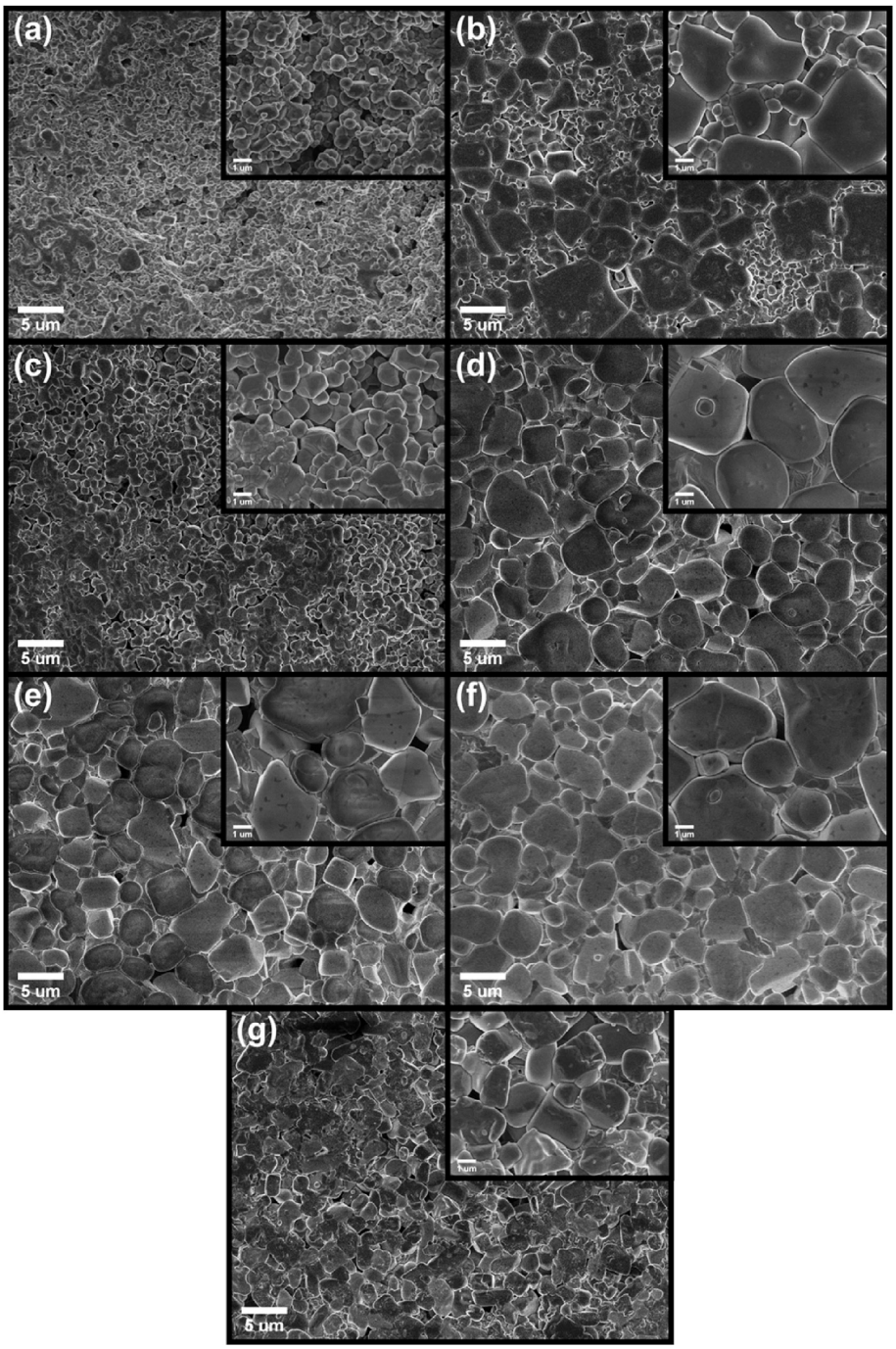

Fig. 5. FE-SEM micrographs of $Ca_2Cu_2Ti_{4-x}Sn_xO_{12}$ ceramic composites for Sn^{4+} substitution with (a) x = 0.0 (b) x = 0.1; (c) x = 0.2; (d) x 2.0; (e) x = 3.8; (f) x = 3.9; (g) x = 4.0. Left inset: High magnification images.

dielectric loss and the frequency [52], different behaviors is noted for the samples with x = 0.0, x = 0.1 and x = 0.2, when compared to samples with x = 3.8, x = 3.9 and x = 4.0. These different behaviors can be associated to polarization mechanisms. The AC conductivity for samples with low Sn^{4+} contents (x = 0.1 and x = 0.2) is frequency independent, but at higher frequencies, the AC conductivity increases, following Jonscher power law behavior [53]. This conductivity behavior is generally due to the hopping of charge carriers in finite clusters frequency. On the other hand, Fig. 7b shows the activation energy (E_a) graphs for a fixed frequency of 1 kHz. The sample with x = 0.1 has a E_a value of 0.46 eV indicating a less conductor behavior and the he sample with x = 2.0 has a E_a value of 0.09 eV implying a high conductivity.

Fig. 8a–b correspond to the activation energies for the grain boundary and the grain respectively. According to the imaginary impedance vs. frequency curves (Fig. S1), the samples with low Sn^{4+} content presented an inflection point at low frequencies associated to the grain boundary. On the other hand, a different behavior is noted for the samples with Sn^{4+} content above of x = 2.0, which presented such inflection at higher frequencies, corresponding to the grain influence. Thus, the samples with x = 0.0, 0.1 and 0.2 presented higher values of activation energy for

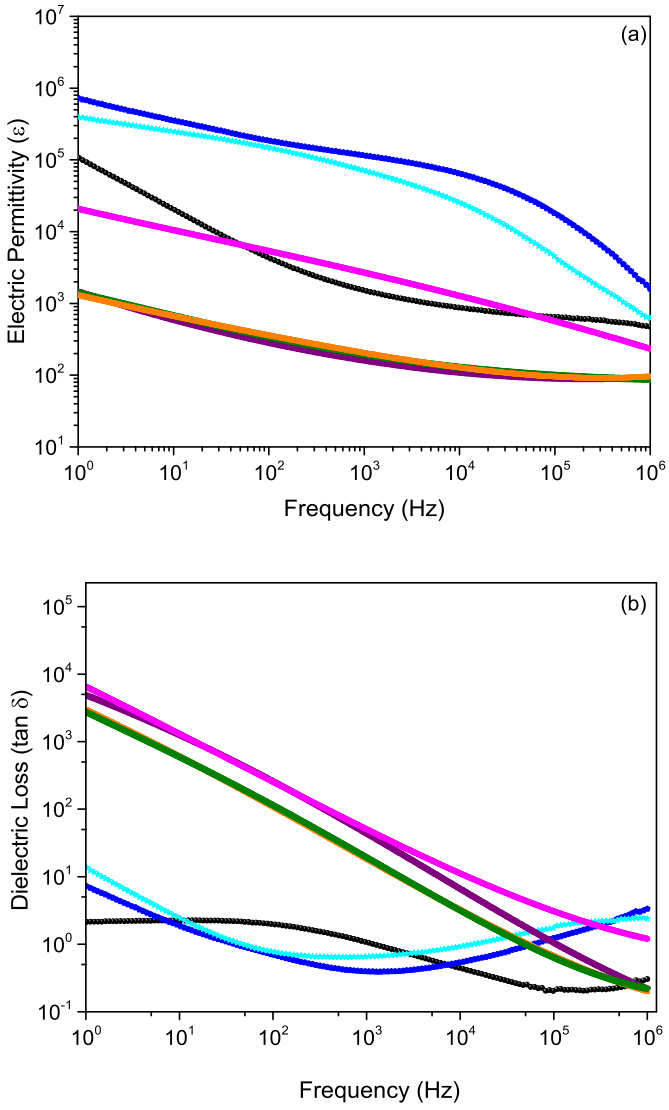

Fig. 6. (a) Electric permittivity (ε′) and (b) dielectric loss (tanδ) as function of frequency of $Ca_2Cu_2Ti_{4-x}Sn_xO_{12}$ ceramic composites.

the grain boundary and very low values for the grain, which explains the high dielectric permittivity, as in agreement with the IBLC model [12,54–57]. In the case of samples with x = 3.8, 3.9 and 4.0, the grain boundary activation energy values were lower when compared to the samples with x = 0.0, x = 0.1 and x = 0.2. This could explained by the segregation of the CuO phase in the grain boundary as already explained by other authors [45,58,59], which occurs due the release of Ti^{4+} from the network. According to the activation energy proposed for the grain boundaries and grains (Fig. 8a–b), it can be noted that the samples with low Sn^{4+} content show low E_a in the grain boundary and high E_a in the grains. These behavior could promoted an increase in the semiconductor character, acting as a resistor. For high Sn^{4+} contents, the activation energy values indicates more insulator grains and grain boundaries more conductives. When the Sn^{4+} contents is x = 2.0, a similar activation energy values for the grain boundary as for the grains, indicates a resistive behavior, independent of the number of grains and grain boundaries.

Fig. 9 shows the current density versus electric field curves for $Ca_2Cu_2Ti_{4-x}Sn_xO_{12}$ ceramic composites. Low Sn^{4+} substituted samples (x = 0.1 and x = 0.2) reveal an abrupt decay of the breakdown electric field (E_b) and lower non-linear coefficient (α), but a slight increasing in the leakage current (I_L). On the other hand, for high Sn^{4+} substituted samples (x = 3.8, 3.9 and 4.0), the non-ohmic response becomes more evident increasing the breakdown electric field (E_b) and the non-linear coefficient (α). New studies are ongoing to better elucidate the varistor response of the SnO_2/$CaSnO_3$/CuO system, mainly, to understand the role of $CaSnO_3$ phase, on which there are no studies about its varistor response. The non-linear coefficient (α) for Sn^{4+} substituted with x = 2.0 is equal to 1.0, indicating an ohmic behavior. As it has been reported, the increase in average grain size leads to huge dielectric permittivity and dielectric loss [60,61]. However, in nonlinear oxide ceramics with Schottky-type grain boundaries, as CCTO [62], there is an increase in the average of grain size, which leads to decrease the breakdown electric field (E_b), as consequence of the decreasing on the number of active potential barriers at the grain boundaries [63].

According to the previous discussion, a proposed model will help to understand the dielectric and non-ohmic properties of low Sn^{4+} substituted samples (x = 0.1 and x = 0.2) into CCTO/CTO composite, as shown in equations (4)–(12).

1. Considering only the output of Ti^{4+} from the lattice:

$$Ca_2Cu_2Ti_4O_{12} \xrightarrow{SnO_2} 2Ca_{ca}^{x} + 2Cu_{cu}^{x} + 4V_{Ti}^{''''} + 12O_O^{x} + 8V_O^{\bullet\bullet} \quad (4)$$

$$CaCu_3Ti_4O_{12} \xrightarrow{SnO_2} Ca_{ca}^{x} + 3Cu_{cu}^{x} + 4V_{Ti}^{''''} + 12O_O^{x} + 8V_O^{\bullet\bullet} \quad (5)$$

$$CaTiO_3 \xrightarrow{SnO_2} Ca_{ca}^{x} + V_{Ti}^{''''} + 3O_O^{x} + 2V_O^{\bullet\bullet} \quad (6)$$

Oxygen vacancies are produced with the release of Ti^{4+} from the structure, which will improve the dielectric permittivity.

2. Sn^{4+} substituted Ti^{4+} sites in CCTO or in the CTO phases.

$$CaCu_3Ti_4O_{12} \xrightarrow{SnO_2} 2Ca_{Ca}^{x} + 3Cu_{Cu}^{x} + 4Sn_{Ti}^{x} + 12O_o^{x} \quad (7)$$

Table 2
Electrical and dielectric parameters for $Ca_2Cu_2Ti_{4-x}Sn_xO_{12}$ ceramic composites.

Sn^{4+} substitution	Impedance ω → 0 (kΩ)	ε′ (1 kHz)	ε′ (10 kHz)	tanδ (1 kHz)	tanδ (10 kHz)	α (1–10 mA)	E_b (V/cm)	Ea_{gb} (eV)	Ea_b (eV)	I_L (μA)
x = 0.0	>1000	2100	873	1.00	0.41	8.0	1200	0.47 ± 0.04	0.04 ± 0.01	210
x = 0.1	180	166381	29168	0.54	0.49	2.0	25	0.58 ± 0.01	0.04 ± 0.01	250
x = 0.2	150	140845	68983	0.71	0.92	2.0	48	0.30 ± 0.03	0.08 ± 0.02	160
x = 2.0	6	3500	1348	210	12.9	1.0	–	0.20 ± 0.05	0.23 ± 0.07	–
x = 3.8	100	210	122	210	6.48	3.0	230	0.21 ± 0.02	0.15 ± 0.01	250
x = 3.9	210	210	122	78	3.05	4.0	420	0.31 ± 0.01	0.15 ± 0.01	340
x = 4.0	210	210	122	78	3.05	4.0	570	0.24 ± 0.01	0.13 ± 0.04	210

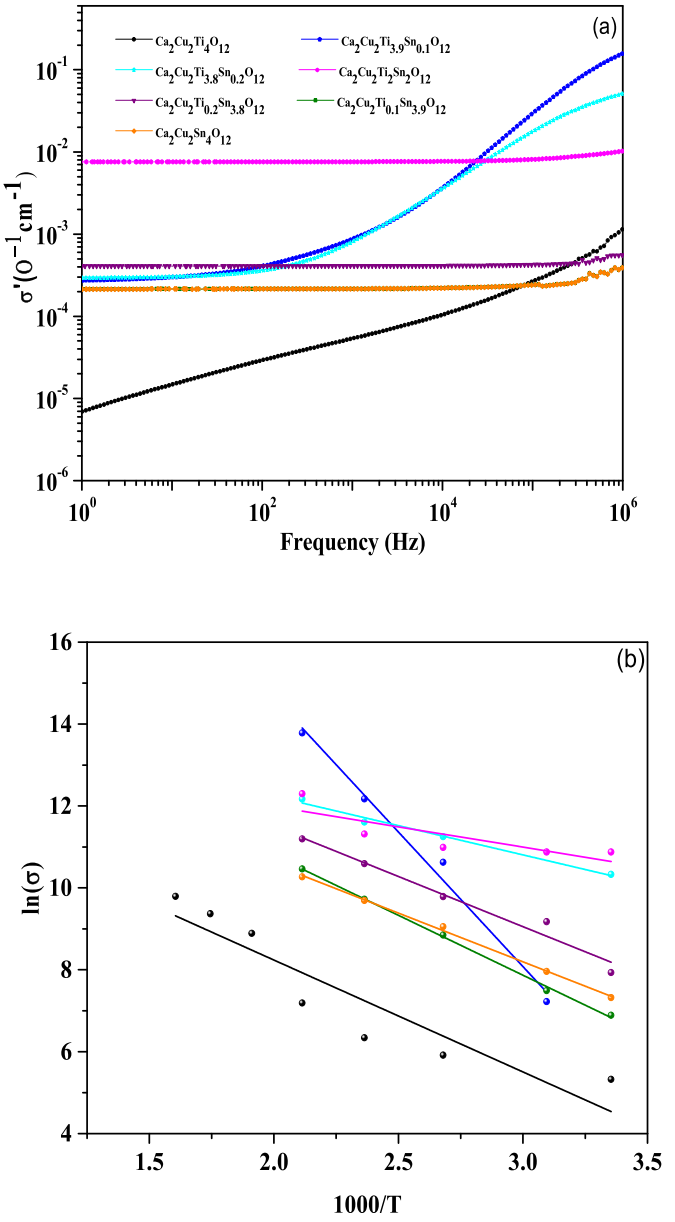

Fig. 7. (a) Conductivity vs. Frequency (b) activation energy for $Ca_2Cu_2Ti_{4-x}Sn_xO_{12}$.

$$CaTiO_3 \xrightarrow{SnO_2} Ca_{ca}^{x} + Sn_{Ti}^{x} + 3O_O^{x} \quad (8)$$

In this case, no electronic defect will be produced associating the high dielectric permittivity with huge grain size. The previous notations described the possibility of the oxygen vacancies formation and the possibility to rule out any kind of point defect. Following, there are no metal vacancies produced:

3. When the Sn^{4+} replaces the Cu^{2+} into the CCTO lattice, produces a decrease in the dielectric property.

$$CaCu_3Ti_4O_{12} \xrightarrow{SnO_2} Ca_{Ca}^{x} + 3Sn_{Cu}^{\bullet\bullet} + 4Ti_{Ti}^{x} + 12O_o^{x} + 3V_{Cu}^{''} \quad (9)$$

4. When Sn^{4+} enters into the CCTO lattice interstitially.

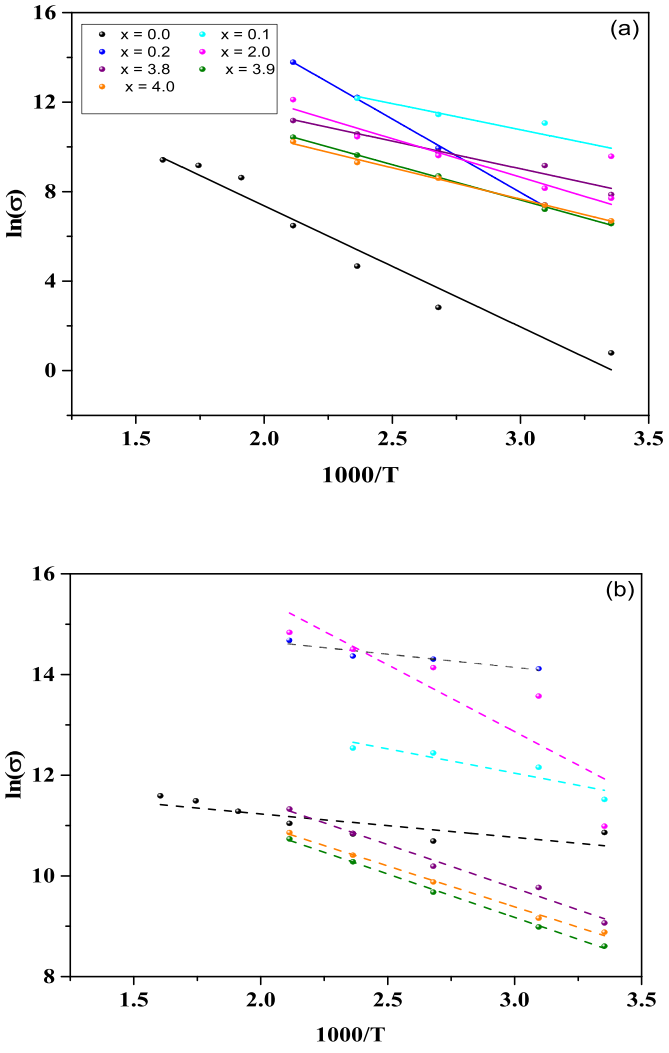

Fig. 8. Activation Energy for (a) grain boundary (b) Grain.

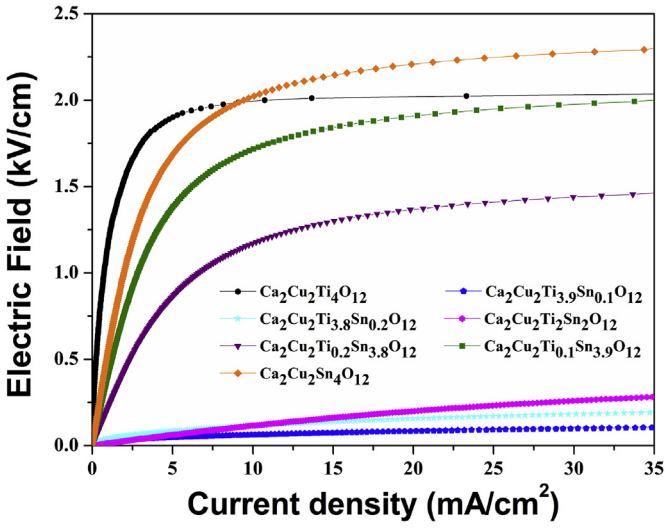

Fig. 9. Density current (J) vs. Electric Field (E) for $Ca_2Cu_2Ti_{4-x}Sn_xO_{12}$.

$$CaCu_3Ti_4O_{12} \xrightarrow{SnO_2} Sn_i^{\bullet\bullet\bullet\bullet} + 3Cu_{Cu}^{x} + 4Ti_{Ti}^{x} + 12O_o^{x} + 2V_{Ca}^{''} \quad (10)$$

$$2CaCu_3Ti_4O_{12} \xrightarrow{SnO_2} 2Ca_{Ca}^{x} + 3Sn_i^{\bullet\bullet\bullet\bullet} + 8Ti_{Ti}^{x} + 24O_o^{x} + 6V_{Cu}^{''} \quad (11)$$

5. When Sn^{4+} enters into the CTO lattice interstitially

$$2CaTiO_3 \xrightarrow{SnO_2} Sn_i^{\bullet\bullet\bullet\bullet} + 2Ti_{Ti}^{x} + 6O_o^{x} + 2V_{Ca}^{''} \quad (12)$$

Equations (9-12) would help to explain the non-ohmic response. However, we conclude that samples with low Sn^{4+} substituted samples (x = 0.1 and 0.2) may be solely governed by the defects reactions present in equations (4)–(8). Besides that, the non-ohmic response of the samples with higher Sn^{4+} substitutions (x = 3.8, 3.9 and 4.0) can be only explained by the SnO_2 phase frequently investigated as varistors [64–66]. However, $CaSnO_3$ has not yet being applied for varistors and CuO which would be a densifying agent in the SnO_2/$CaSnO_3$/CuO system [37]. Therefore, we infer that at low Sn^{4+}concentrations, more oxygen vacancies were produced as a consequence of Ti^{4+} output from the lattice, which increases the lattice parameters (see Table S1). On the other hand, Cu^{2+} is replacing Sn^{4+} into the CCTO lattice producing Cu^{2+} vacancy, which reduced the dielectric properties significantly. Ribeiro et al. have reported that the substitution of Sn^{4+} into pure CCTO ceramics leads to an improvement in the non-ohmic behavior, which it may indicate that low substitution of Sn^{4+} (x = 0.1 and 0.2) leads to an increasing in the potential barrier height at the CCTO grain boundaries [67]. Besides, it is well known in the literature that relaxation processes in oxide ceramics at low frequency are normally related to the grain boundary contribution [68]. As shown in Fig. 10, it can be clearly observed one impedance arc as a function of the Sn^{4+} contents in the CCTO/CTO samples which suggest a relaxation process at low frequency (Fig. S1). On the other hand, for x = 0.0, the impedance arc is not full in the analyzed frequency range. Also the impedance for $\omega \rightarrow 0$ (Table 2), normally related to the grain boundary resistance, is much lower for small concentrations than for the x = 0.0 [69]. Such model can be explained based on the Internal Barrier Layer Capacitance (IBLC) revealing a huge increase in the dielectric permittivity. On the other hand, the dielectric characteristics of the high Sn^{4+} substituted samples (x = 3.8; 3.9 and 4.0) were expected as a consequence of multiple phases, once tin-based ceramics are normally well-known as good non-ohmic ceramics [70]. Furthermore, the studies have revealed that the non-linear behavior can be improved by controlling the characteristics of the grain boundary using different approaches, such as thermal treatment under oxygen atmosphere, doping with different oxidation states in order to promote defects in the grain boundary region affecting the conduction behavior at the grain boundary [70,71]. The initial results indicate that tin-based ceramic composites follow the main characteristics of the conventional non-ohmic materials [28], for instance, the breakdown electric field increases as the average grain size decreases. Those interesting phenomena need to be further studied.

4. Conclusion

$Ca_2Cu_2Ti_{4-x}Sn_xO_{12}$ ceramic composites were prepared by solid-state method. XRD results indicated that two different groups of ceramic composites were obtained depending on the level of ionic substitution. The microstructure results have shown that each ceramic composite has its densification and grain growth processes controlled by different sintering mechanisms. This study also revealed that low Sn^{4+} substitutions (x = 0.1 and 0.2) showed the AC conductivity increased, following Jonscher power law behavior, associated to hopping of charge carriers in finite clusters frequency.

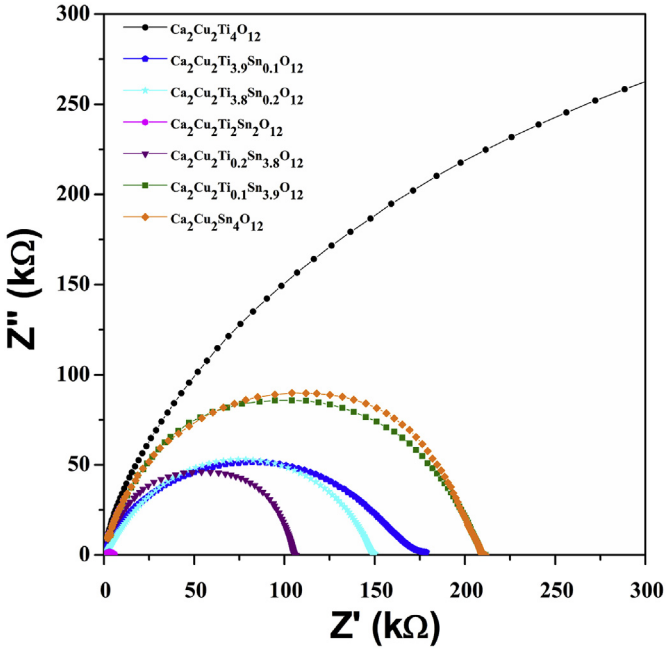

Fig. 10. Impedance spectra of $Ca_2Cu_2Ti_{4-x}Sn_xO_{12}$ ceramic composite.

That makes more effective the improvement in the dielectric property, while the non-ohmic property was enhanced with higher Sn^{4+} substitutions (x = 3.8, 3.9 and 4.0), excepts to samples with x = 2.0, that showed an ohmic behavior. The activation energy showed that at low Sn^{4+} levels, the grains are conductive while the grain boundary is insulator. However, for higher Sn^{4+} concentrations, the CuO phase is segregated at the grain boundary, leading to a more conductive sample. In summary, this work indicates that low amounts of Sn^{4+} are effective to enhance the dielectric performance of CCTO/CTO based ceramics and points out to a new kind of approach to improve the performance of non-ohmic tin-based ceramics.

Acknowledgements

The authors gratefully acknowledge the National Council for Scientific – (CAPES) and also thanks Anderson André Felix for their contribution to the development of this work.

Appendix A. Supplementary data

Supplementary data related to this article can be found at https://doi.org/10.1016/j.jallcom.2017.11.089.

References

[1] H. Eun, S. Choi, Y. Hong, S. Yoo, Improved dielectric properties of the $CaCu_3Ti_4O_{12}$ composites using BaTiO 3 -coated powder as precursor, J. Alloys. Compd. 610 (2014) 594–599, https://doi.org/10.1016/j.jallcom.2014.04.215.
[2] M.O. Orlandi, M.A. Ramirez, C.R. Foschini, A.A. Felix, J.A. Varela, Giant dielectric constant materials and their aplications, in: M.A. Aegerter, M. Prassas (Eds.), Sol-gel Processing for Conventional and Alternative Energy, New York, n.d.: pp. 123–146. doi:10.1007/978-1-4614-1957-0.
[3] A.A. Felix, J.L.M. Rupp, J.A. Varela, M.O. Orlandi, Multi-functional properties of $CaCu_3Ti_4O_{12}$ thin films, J. Appl. Phys. 112 (2012) 1–7, https://doi.org/10.1063/1.4751344.
[4] C.C. Homes, T. Vogt, S.M. Shapiro, S. Wakimoto, A.P. Ramirez, Optical response of high-dielectric-constant perovskite-related oxide, Science (New York, N.Y.) 293 (2001) 673–676, https://doi.org/10.1126/science.1061655.
[5] M.A. Subramanian, D. Li, N. Duan, B.A. Reisner, A.W. Sleight, High dielectric constant in $ACu_3Ti_4O_{12}$ and $ACu_3Ti_3FeO_{12}$ phases, J. Solid State Chem. 151 (2000) 323–325, https://doi.org/10.1006/jssc.2000.8703.

[6] A.P. Ramirez, M.A. Subramanian, M. Gardel, G. Blumberg, D. Li, T. Vogt, S.M. Shapiro, Giant dielectric constant response in a copper-titanate, Solid State Commun. 115 (2000) 217–220, https://doi.org/10.1016/S0038-1098(00)00182-4.

[7] P.R. Bueno, M.A. Ramírez, J.A. Varela, E. Longo, P.R. Bueno, M.A. Ramírez, J.A. Varela, E. Longo, Dielectric spectroscopy analysis of Dielectric spectroscopy analysis of $CaCu_3Ti_4O_{12}$ polycrystalline systems, Appl. Phys. Lett. (2006), https://doi.org/10.1063/1.2386916, 191117.

[8] B.A. Bender, M.-J. Pan, The effect of processing on the giant dielectric properties of $CaCu_3Ti_4O_{12}$, Mater. Sci. Eng. B 117 (2005) 339–347, https://doi.org/10.1016/j.mseb.2004.11.019.

[9] X. Ouyang, M. Habib, P. Cao, S. Wei, Z. Huang, W. Zhang, W. Gao, Enhanced extrinsic dielectric response of TiO_2 modified $CaCu_3Ti_4O_{12}$ ceramics, Ceram. Int. 41 (2015) 13447–13454, https://doi.org/10.1016/j.ceramint.2015.07.133.

[10] S. Rhouma, S. Senda, C. Autret, S. De Almeida-Didry, M.A. El-Shaer, Ade, Comparative studies of pure, Sr-doped, Ni-doped and co-doped $CaCu_3Ti_4O_{12}$ ceramics: enhancement of dielectric properties, J. Alloys. Compd. 717 (2017) 121–126, https://doi.org/10.1016/j.jallcom.2017.05.053.

[11] J. Boonlakhorn, P. Kidkhunthod, P. Thongbai, A novel approach to achieve high dielectric permittivity and low loss tangent in $CaCu_3Ti_4O_{12}$ ceramics by co-doping with Sm^{3+} and Mg^{2+} ions, J. Eur. Ceram. Soc. 35 (2015) 3521–3528, https://doi.org/10.1016/j.jeurceramsoc.2015.06.008.

[12] A.K. Thomas, K. Abraham, J. Thomas, K.V. Saban, Structural and dielectric properties of A- and B-sites doped $CaCu_3Ti_4O_{12}$ ceramics, Ceram. Int. 41 (2015) 10250–10255, https://doi.org/10.1016/j.ceramint.2015.04.138.

[13] K. Meeporn, T. Yamwong, S. Pinitsoontorn, V. Amornkitbamrung, P. Thongbai, Grain size independence of giant dielectric permittivity of $CaCu_3Ti_{4-x}Sc_xO_{12}$ ceramics, Ceram. Int. 40 (2014) 1–10, https://doi.org/10.1016/j.ceramint.2014.07.118.

[14] W.C. Ribeiro, R.G.C. Araújo, P.R. Bueno, The dielectric suppress and the control of semiconductor non-Ohmic feature of by means of tin doping the dielectric suppress and the control of semiconductor non-Ohmic feature of $CaCu_3Ti_4O_{12}$ by means of tin doping, Appl. Phys. Lett. (2011) 98–101, https://doi.org/10.1063/1.3574016, 132906.

[15] R. Schmidt, D.C. Sinclair, Anomalous increase of dielectric permittivity in Sr-Doped CCTO ceramics $Ca_{1-x}Sr_x$ $Cu_3Ti_4O_{12}$ ($0.0 \leq x \leq 0.2$), Chem. Mater. 22 (2010) 6–8, https://doi.org/10.1021/cm903220z.

[16] W. Li, S.Y. Qiu, N. Chen, B.F. Liu, G.P. Du, Enhanced dielectric properties and sinterability of $CaCu_3Ti_4O_{12}$ ceramics by Sr^{2+} doping, Phys. B Condens. Matter 405 (2010) 1193–1196, https://doi.org/10.1016/j.physb.2009.11.038.

[17] M.A. Ramírez, P.R. Bueno, R. Tararam, A.A. Cavalheiro, E. Longo, J.A. Varela, Evaluation of the effect of the stoichiometric ratio of Ca/Cu on the electrical and microstructural properties of the $CaCu_3Ti_4O_{12}$ polycrystalline system, J. Phys. D Appl. Phys. 42 (2009) 185503, https://doi.org/10.1088/0022-3727/42/18/185503.

[18] J. Boonlakhorn, P. Kidkhunthod, B. Putasaeng, P. Thongbai, Significantly improved non-Ohmic and giant dielectric properties of $CaCu_{3-x}Zn_xTi_4O_{12}$ ceramics by enhancing grain boundary response, Ceram. Int. 43 (2017) 2705–2711, https://doi.org/10.1016/j.ceramint.2016.11.089.

[19] G. Du, F. Wei, W. Li, N. Chen, Co-doping effects of A-site Y^{3+} and B-site Al^{3+} on the microstructures and dielectric properties of $CaCu_3Ti_4O_{12}$ ceramics, J. Eur. Ceram. Soc. 37 (2017) 4653–4659, https://doi.org/10.1016/j.jeurceramsoc.2017.06.046.

[20] S.-Y. Chung, I.-D. Kim, S.-J.L. Kang, Strong nonlinear current-voltage behaviour in perovskite-derivative calcium copper titanate, Nat. Mater. 3 (2004) 774–778, https://doi.org/10.1038/nmat1238.

[21] D. Xu, L. Shi, Z. Wu, Q. Zhong, X. Wu, Microstructure and electrical properties of ZnO-Bi_2O_3-based varistor ceramics by different sintering processes, J. Eur. Ceram. Soc. 29 (2009) 1789–1794, https://doi.org/10.1016/j.jeurceramsoc.2008.10.020.

[22] M.A. Ramírez, P.R. Bueno, J.A. Varela, E. Longo, Non-Ohmic and dielectric properties of a Non-Ohmic and dielectric properties of a $Ca_2Cu_2Ti_4O_{12}$ polycrystalline, Appl. Phys. Lett. 89 (2006) 1–4, https://doi.org/10.1063/1.2393122.

[23] P. Thongbai, J. Jumpatam, B. Putasaeng, T. Yamwong, Microstructural evolution and Maxwell – Wagner relaxation in $Ca_2Cu_2Ti_{4-x}Zr_xO_{12}$: the important clue to achieve the origin of the giant dielectric behavior, Mater. Res. Bull. 60 (2014) 695–703, https://doi.org/10.1016/j.materresbull.2014.09.045.

[24] M.A. Ramírez, W. Bassi, P.R. Bueno, E. Longo, J.A. Varela, Comparative degradation of ZnO- and SnO_2 -based polycrystalline non-ohmic devices by current pulse stress, J. Phys. D Appl. Phys. 41 (2008) 122002, https://doi.org/10.1088/0022-3727/41/12/122002.

[25] M.A. Ramírez, A.Z. Simões, M.A. Márquez, Y. Maniette, A.A. Cavalheiro, J.A. Varela, Characterization of ZnO-degraded varistors used in high-tension devices, Mater. Res. Bull. 42 (2007) 1159–1168, https://doi.org/10.1016/j.materresbull.2006.09.001.

[26] S.K. Abbas, S. Atiq, S. Riaz, S. Naseem, Thermally activated variations in conductivity and activation energy in $SrMnO_3$, J. Mater. Sci. Mater. Electron. 28 (2017) 7171–7176, https://doi.org/10.1007/s10854-017-6397-5.

[27] Q. Zheng, H. Fan, C. Long, Microstructures and electrical responses of pure and chromium-doped $CaCu_3Ti_4O_{12}$ ceramics, J. Alloys. Compd. 511 (2012) 90–94, https://doi.org/10.1016/j.jallcom.2011.09.002.

[28] D.R. Clarke, Varistor ceramics, J. Am. Ceram. Soc. 82 (1999) 485–502.

[29] D. Xu, K. He, R. Yu, L. Jiao, H. Yuan, X. Sun, G. Zhao, H. Xu, X. Cheng, Effect of $AETiO_3$ (AE = Mg, Ca, Sr) doping on dielectric and varistor characteristics of CaCu3Ti4O12 ceramic prepared by the sol-gel process, J. Alloys. Compd. 592 (2014) 220–225, https://doi.org/10.1016/j.jallcom.2013.12.264.

[30] X.G. Li, Y. Lv, B.G. Ma, W.Q. Wang, S.W. Jian, Decomposition kinetic characteristics of calcium carbonate containing organic acids by TGA, Am. J. Chem. 3 (2013), https://doi.org/10.1016/j.arabjc.2013.09.026.

[31] C. Huang, X. Wang, X. Liu, M. Tian, T. Zhang, Extensive analysis of the formation mechanism of BaSnO3 by solid state reaction between $BaCO_3$ and SnO_2, J. Eur. Ceram. Soc. 36 (2016) 583–592, https://doi.org/10.1016/j.jeurceramsoc.2015.11.001.

[32] A.O. Merkushkin, T. Aung, Z.E.U. Mo, Ceramics based on free zirconates, titanates, and stannates, Glass Ceram. 67 (2011) 16–19.

[33] G. Pfaff, Preparation and characterization of the strontium stannates $SrSnO_3$ and Sr_2SnO_4, J. Mater. Sci. 5 (2000) 3017–3021.

[34] T.B. Adams, D.C. Sinclair, A.R. West, Decomposition reactions in $CaCu_3Ti_4O_{12}$ ceramics, J. Am. Ceram. Soc. 89 (2006) 2833–2838, https://doi.org/10.1111/j.1551-2916.2006.01174.x.

[35] A.A. Felix, V.D.N. Bezzon, M.O. Orlandi, D. Vengust, M. Spreitzer, E. Longo, D. Suvorov, J.A. Varela, Role of oxygen on the phase stability and microstructure evolution of $CaCu_3Ti_4O_{12}$ ceramics, J. Eur. Ceram. Soc. 37 (2017) 129–136, https://doi.org/10.1016/j.jeurceramsoc.2016.07.039.

[36] J. Jumpatam, B. Putasaeng, T. Yamwong, P. Thongbai, S. Maensiri, Microstructural evolution and strongly enhanced dielectric response in Sn-doped $CaCu_3Ti_4O_{12}/CaTiO_3$ ceramic composites, Mater. Res. Bull. 77 (2016) 178–184, https://doi.org/10.1016/j.materresbull.2016.01.031.

[37] C.M. Wang, J.F. Wang, H.C. Chen, W. Bin Su, G.Z. Zang, P. Qi, M.L. Zhao, Effects of CuO on the grain size and electrical properties of SnO_2-based varistors, Mater. Sci. Eng. B: Solid-State Materials for Advanced Technology 116 (2005) 54–58, https://doi.org/10.1016/j.mseb.2004.09.009.

[38] J. Lalande, R. Ollitrault-fichet, P. Boch, Sintering behaviour of CuO-doped SnO_2, J. Eur. Ceram. Soc. 20 (2000).

[39] P.R. Bueno, R. Tararan, R. Parra, Evaluation of the effect of the stoichiometric ratio of Ca/Cu on the electrical and microstructural properties of the $CaCu_3Ti_4O_{12}$ polycrystalline system, J. Phys D. Appl. Phys. 42 (2009) 8, https://doi.org/10.1088/0022–3727/42/18/185503.

[40] N. Dolet, J. Heintz, M. Onillon, J. Bonnet, Densification of 0.99SnO2-0. 01CuO Mixture: Evidence for Liquid Phase Sintering, 9 (n.d.) 19–25.

[41] N. Dolet, J.M. Heintz, L. Rabardel, M. Onillon, P. Bonnet, Sintering mechanisms of 0.99SnO2-0.01CuO mixtures, J. Mater. Sci. 30 (1995) 365–368.

[42] P. Thongbai, B. Putasaeng, T. Yamwong, S. Maensiri, Improved dielectric and non-ohmic properties of Ca2Cu2Ti4O12 ceramics prepared by a polymer pyrolysis method, J. Alloys. Compd. 509 (2011) 7416–7420, https://doi.org/10.1016/j.jallcom.2011.04.052.

[43] J. Jumpatam, P. Thongbai, B. Kongsook, T. Yamwong, S. Maensiri, High permittivity, low dielectric loss, and high electrostatic potential barrier in Ca2Cu2Ti4O12 ceramics, Mater. Lett. 76 (2012) 40–42, https://doi.org/10.1016/j.matlet.2012.02.054.

[44] X.J. Luo, Y.S. Liu, C.P. Yang, S.S. Chen, S.L. Tang, K. Bärner, Oxygen vacancy related defect dipoles in CaCu 3 Ti 4 O 12: detected by electron paramagnetic resonance spectroscopy, J. Eur. Ceram. Soc. 35 (2015) 2073–2081, https://doi.org/10.1016/j.jeurceramsoc.2015.01.024.

[45] M.J. Abu, J.J. Mohamed, M.F. Ain, Z.A. Ahmad, Phase structure, microstructure and broadband dielectric response of Cu nonstoichiometry CaCu3Ti4O12 ceramic, J. Alloys. Compd. 683 (2016) 579–589, https://doi.org/10.1016/j.jallcom.2016.04.318.

[46] L. Singh, U.S. Rai, K.D. Mandal, N.B. Singh, Progress in the growth of CaCu3-Ti4O12 and related functional dielectric perovskites, Prog. Cryst. Growth Char. Mater. 60 (2014) 15–62, https://doi.org/10.1016/j.pcrysgrow.2014.04.001.

[47] L. Singh, U.S. Rai, K.D. Mandal, B.C. Sin, H. Il Lee, H. Chung, Y. Lee, Comparative dielectric studies of nanostructured BaTiO3, CaCu3Ti4O12 and 0.5BaTiO3· 0.5$CaCu_3Ti_4O_{12}$ nano-composites synthesized by modified sol-gel and solid state methods, Mater. Char. 96 (2014) 54–62, https://doi.org/10.1016/j.matchar.2014.07.019.

[48] A.K. Rai, K.D. Mandal, D. Kumar, O. Parkash, Characterization of nickel doped CCTO: $CaCu_{2.9}Ni_{0.1}Ti_4O_{12}$ and $CaCu_3Ti_{3.9}Ni_{0.1}O_{12}$ synthesized by semi-wet route, J. Alloys. Compd. 491 (2010) 507–512, https://doi.org/10.1016/j.jallcom.2009.10.247.

[49] Z. Li, G. Xu, Y. Li, A. Sun, L. Duan, J. Jiang, P. Cui, Dielectric and non-ohmic properties of $Bi_xNa_{1-x}Nb_2O_{5.5\ +\ x}$ ceramics, J. Alloys. Compd. 481 (2009) 6–8, https://doi.org/10.1016/j.jallcom.2009.02.148.

[50] M. Mitsugi, S. Asanuma, Origin of colossal dielectric response of $CaCu_3Ti_4O_{12}$ studied by using $CaTiO_3/CaCu_3Ti_4O_{12}/CaTiO_3$ multilayer thin films, Appl. Phys. 242904 (2007) 1–4, https://doi.org/10.1063/1.2748854.

[51] L. Singh, I.W. Kim, B.C. Sin, K.D. Mandal, U.S. Rai, A. Ullah, H. Chung, Y. Lee, Dielectric studies of a nano-crystalline $CaCu_{2.90}$ $Zn_{0.10}$ Ti_4 O_{12} electroceramic by one pot glycine assisted synthesis from inexpensive TiO_2 for energy storage capacitors, RSC Adv. 4 (2014) 52770–52784, https://doi.org/10.1039/C4RA08915D.

[52] R. Kashyap, O.P. Thakur, R.P. Tandon, Study of structural, dielectric and electrical conduction behaviour of Gd substituted $CaCu_3Ti_4O_{12}$ ceramics, Ceram. Int. 38 (2012) 3029–3037, https://doi.org/10.1016/j.ceramint.2011.11.085.

[53] A.K. Jonscher, Dielectric relaxation in solids, J. Phys. D Appl. Phys. 32 (1999) R57–R70, https://doi.org/10.1088/0022-3727/32/14/201.

[54] V. Brizé, G. Gruener, J. Wolfman, K. Fatyeyeva, M. Tabellout, M. Gervais, F. Gervais, Grain size effects on the dielectric constant of $CaCu_3Ti_4O_{12}$ ceramics, Mater. Sci. Eng. B 129 (2006) 135–138, https://doi.org/10.1016/j.mseb.2006.01.004.

[55] C.R. Foschini, R. Tararam, A.Z. Simões, M. Cilense, E. Longo, J.A. Varela, $CaCu_3Ti_4O_{12}$ thin films with non-linear resistivity deposited by RF-sputtering, J. Alloys. Compd. 574 (2013) 604–608, https://doi.org/10.1016/j.jallcom.2013.05.216.

[56] J. Jumpatam, B. Putasaeng, T. Yamwong, P. Thongbai, S. Maensiri, Enhancement of giant dielectric response in Ga-doped $CaCu_3Ti_4O_{12}$ ceramics, Ceram. Int. 39 (2013) 1057–1064, https://doi.org/10.1016/j.ceramint.2012.07.027.

[57] J. Jumpatam, B. Putasaeng, T. Yamwong, P. Thongbai, S. Maensiri, Microstructural evolution and strongly enhanced dielectric response in Sn-doped $CaCu_3Ti_4O_{12}/CaTiO_3$ ceramic composites, Mater. Res. Bull. 77 (2016) 178–184, https://doi.org/10.1016/j.materresbull.2016.01.031.

[58] T.T. Fang, L.T. Mei, H.F. Ho, Effects of Cu stoichiometry on the microstructures, barrier-layer structures, electrical conduction, dielectric responses, and stability of $CaCu_3Ti_4O_{12}$, Acta Mater. (2006), https://doi.org/10.1016/j.actamat.2006.02.037.

[59] T. Li, K. Fang, J. Hao, Y. Xue, Z. Chen, The effect of Ca-rich on the electric properties of Ca $_{1+x}$ Cu $_{3-x}$ Ti $_4$ O $_{12}$ polycrystalline system, Mater. Sci. Eng. B 176 (2010) 171–176, https://doi.org/10.1016/j.mseb.2010.10.010.

[60] S. Rachna, S. Bhattacharyya, S.M. Gupta, Dielectric properties and ac-conductivity analysis of $Bi_{3.25}La_{0.75}Ti_3O_{12}$ ceramic using impedance spectroscopy, J. Phys. Chem. Solid. 69 (2008) 822–829, https://doi.org/10.1016/j.jpcs.2007.09.004.

[61] P.R. Bueno, R. Tararan, R. Parra, E. Joanni, M.A. Ramirez, W.C. Ribeiro, E. Longo, A polaronic stacking fault defect model for $CaCu_3Ti_4O_{12}$ material: an approach for the origin of the huge dielectric constant and semiconducting coexistent features, J. Phys D. Appl. Phys. 55404 (2009) 9, https://doi.org/10.1088/0022–3727/42/5/055404.

[62] A.A. Felix, M.O. Orlandi, J.A. Varela, Schottky-type grain boundaries in CCTO ceramics, Solid State Commun. 151 (2011) 1377–1381, https://doi.org/10.1016/j.ssc.2011.06.012.

[63] P.R. Bueno, M.O. Orlandi, L.G. Simões, E.R. Leite, E. Longo, A. Cerri, Nonohmic behavior of SnO_2 -MnO polycrystalline ceramics. Correlations between microstructural morphology and nonohmic features, J. Appl. Phys. 96 (2004) 2693–2700, https://doi.org/10.1063/1.1772874.

[64] S. Ma, Z. Xu, R. Chu, J. Hao, W. Li, L. Cheng, G. Li, Influence of SnO_2 on $ZnO–Bi_2O_3–Co_2O_3$ based varistor ceramics, Ceram. Int. 41 (2015) 12490–12494, https://doi.org/10.1016/j.ceramint.2015.06.004.

[65] M.A. Ponce, M.A. Ramírez, R. Parra, C. Malagú, M.S. Castro, P.R. Bueno, J.A. Varela, Influence of degradation on the electrical conduction process in ZnO and SnO_2-based varistors, J. Appl. Phys. 108 (2010), https://doi.org/10.1063/1.3490208.

[66] V.P.B. Marques, M. Cilense, P.R. Bueno, M.O. Orlandi, J.A. Varela, E. Longo, Qualitative evaluation of active potential barriers in SnO_2-based polycrystalline devices by electrostatic force microscopy, Appl. Phys. A 87 (2007) 793–796, https://doi.org/10.1007/s00339-007-3922-z.

[67] W.C. Ribeiro, R.G.C. Araújo, P.R. Bueno, The dielectric suppress and the control of semiconductor non-Ohmic feature of $CaCu_3Ti_4O_{12}$ by means of tin doping, Appl. Phys. Lett. 98 (2011) 1–4, https://doi.org/10.1063/1.3574016.

[68] J.R. Macdonald, W.R. Kenan, Impedance Spectroscopy: Emphasizing Solid Materials and Systems, 1987.

[69] P.R. Bueno, M.A. Santos, M.A. Ramírez, R. Tararam, E. Longo, J.A. Varela, Relationship between grain-boundary capacitance and bulk shallow donors in SnO_2 polycrystalline semiconductor, Phys. Status Solidi A 205 (2008) 1694–1698, https://doi.org/10.1002/pssa.200723355.

[70] S.A. Pianaro, P.R. Bueno, E. Longo, J.A. Varela, A new SnO_2-based varistor system, J. Mater. Sci. Lett. 14 (1995) 692–694, https://doi.org/10.1007/BF00253373.

[71] P. Meng, J. Hu, H. Zhao, J. He, High voltage gradient and low residual-voltage ZnO varistor ceramics tailored by doping with In_2O_3 and Al_2O_3, Ceram. Int. 42 (2016) 19437–19440, https://doi.org/10.1016/j.ceramint.2016.09.032.